

## Wind-induced responses and equivalent static wind loads of tower-blade coupled large wind turbine system

S.T. Ke<sup>\*1</sup>, T.G. Wang<sup>1a</sup>, Y.J. Ge<sup>2b</sup> and Y. Tamura<sup>3c</sup>

<sup>1</sup>*Jiangsu Key Laboratory of Hi-Tech Research for Wind Turbine Design, Nanjing University of Aeronautics and Astronautics, 29 Yudao Road, Nanjing 210016, China*

<sup>2</sup>*State Key Laboratory for Disaster Reduction in Civil Engineering, Tongji University, 1239 Siping Road, Shanghai 200092, China*

<sup>3</sup>*Center of Wind Engineering Research, Tokyo Polytechnic University, 1583 Iiyama, Atsugi, Kanagawa 243-0297, Japan*

*(Received August 31, 2013, Revised May 1, 2014, Accepted May 5, 2014)*

**Abstract.** This study aimed to develop an approach to accurately predict the wind models and wind effects of large wind turbines. The wind-induced vibration characteristics of a 5 MW tower-blade coupled wind turbine system have been investigated in this paper. First, the blade-tower integration model was established, which included blades, nacelle, tower and the base of the wind turbine system. The harmonic superposition method and modified blade element momentum theory were then applied to simulate the fluctuating wind field for the rotor blades and tower. Finally, wind-induced responses and equivalent static wind loads (ESWL) of the system were studied based on the modified consistent coupling method, which took into account coupling effects of resonant modes, cross terms of resonant and background responses. Furthermore, useful suggestions were proposed to instruct the wind resistance design of large wind turbines. Based on obtained results, it is shown from the obtained results that wind-induced responses and ESWL were characterized with complicated modal responses, multi-mode coupling effects, and multiple equivalent objectives. Compared with the background component, the resonant component made more contribution to wind-induced responses and equivalent static wind loads at the middle-upper part of the tower and blades, and cross terms between background and resonant components affected the total fluctuation responses, while the background responses were similar with the resonant responses at the bottom of tower.

**Keywords:** large wind turbine system; fluctuating wind field; modified blade element momentum theory; wind-induced response; equivalent static wind load

### 1. Introduction

A distinctive feature of horizontal axis wind turbine systems is that the blades, nacelle, generator and other components are placed at the top of the high and slender tower. The wind

---

\*Corresponding author, Associate Professor, E-mail: keshitang@163.com

<sup>a</sup>Professor, E-mail: tggwang@nuaa.edu.cn

<sup>b</sup>Professor, E-mail: yaojunge@tongji.edu.cn

<sup>c</sup>Professor, E-mail: yukio@arch.t-kougei.ac.jp

turbine system has features like light weight, small damping, low natural vibration frequency and dense distribution, which belongs to the typical wind-sensitive structure (Tarp 2002, Agarwal 2009). The blade of the large wind turbine system becomes much longer with the rotor diameter reaching the magnitude of one hundred metres. Meanwhile, the long blades can be easily deformed and coupled with the powerful wind loads, which could cause swinging and warping in the blade, even the wind-induced resonant destruction or vibration fatigue of the tower (Petrini *et al.* 2010). To ensure the safety performance of the large wind turbine system, the analysis of dynamic responses under random wind loads is crucial in the design of wind turbine system. Especially, the study of accurate fluctuating wind field simulation and reasonable equivalent static wind load (ESWL) model for large wind turbine systems is significant for the wind-resistant design.

In earlier relevant studies, the wind turbine system was modeled as a system with single degree of freedom by Tempel (2002), and dynamic characteristics of the wind turbine system and single wind vibration coefficient were then obtained. However, a model with single degree of freedom cannot accurately reveal the wind-induced response characteristics of wind turbine tower. Stochastic dynamic responses of the blade were analyzed by the classical random vibration theory (Duquette *et al.* 2003). In this theory the vibration mechanism of blade was explained clearly, but the wind-induced vibration responses of the tower itself had not been considered yet. The structural model was extended to the whole wind turbine system (Burton 2011), and dynamic response characteristics based on frequency domain were analyzed, but ESWLs of the wind turbine system were not given. The analyzing method of dynamic responses in the wind turbine system based on time domain was proposed by Cheng (2002), Karimirad and Moan (2011), in which method the randomness of fluctuating wind was considered, but the calculation based on this method was randomly convergent and not efficient enough. The dynamic response of the wind turbine system considering the bladed rotational effect was analyzed (Murtagh 2005, Li *et al.* 2011) without involvement of the wind-induced vibration mechanism and ESWLs.

In view of the above researches, to analyze the wind turbine system accurately, in this paper, the “blade-nacelle-tower-base” integration model of a 5 MW wind turbine system was innovatively established. The speed time series in the wind field for the rotor blades and tower were then simulated based on the harmonic superposition method and modified blade element-momentum theory, which took into account the rotational effect and tower-blade model and aerodynamic interaction effects. Finally, the wind-induced responses and ESWLs of the tower-blade system were calculated using the modified consistent coupling method. Furthermore, useful suggestions were proposed to instruct the wind resistance design of large wind turbine systems.

## 2. Integration model of tower-blade system

The model was built based on the 5MW wind turbine system with three wind blades, which model was developed by Nanjing University of Aeronautics and Astronautics. The tower is 124 m high with the bottom is 4.8 m in diameter, and 150 mm in thickness and the top is 2.6 m in diameter and 60 mm in thickness, the thickness of the tower decreases linearly from the bottom to the top. The nacelle is 12 m in length, 4.6 m in width, 4.2 m in height, with a total mass of  $140.0 \times 10^3$  Kg. The diameter of the wind blade is 120 m, the width of blade is 2.4 m, the thickness is 0.38 m, the length of it is 60 m, the yaw angle is zero degrees, the rated speed is 17.0 r/min.

The blade-nacelle-tower-base integration model of wind turbine system was established based on ANSYS. Both the wind blade and the tower body were simulated by the element of SHELL91;

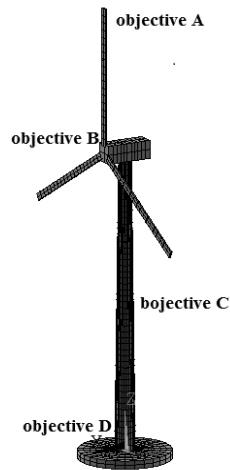


Fig. 1 The integration model of the wind turbine tower-rotor system

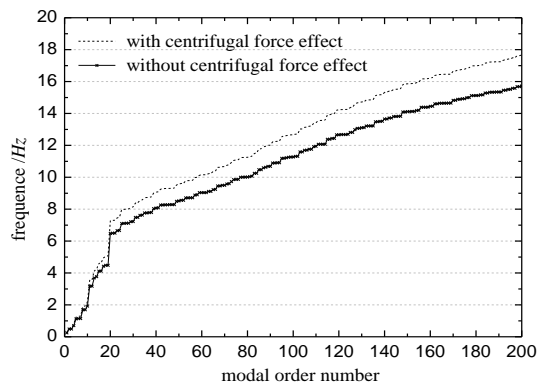


Fig. 2 Scatter gram of natural frequencies in the integration model

the nacelle and its internal structure were simulated as a whole by the element of BEAM189, the circle raft foundation was simulated by the element of SOLID65. The base is 1.8 m high and has a diameter of 10m. It's assumed that the bottom of the foundation was consolidated, without consideration of the soil-structure interaction. All the components were connected together by the command of multi-element coupling to form an integration model. Considering both the efficiency and precision of the equilibrium principle, the model was divided into 6486 elements (as shown in Fig. 1). The centrifugal force generated by the rotation of the wind blades was exerted on the wind blades previously as the pre-stressing force during the modal analysis to take into account the effect of centrifugal force.

According to the norm of GL-2005 Rules and Guidelines IV (Germanischer Lloyd 2005), the stability and strength of the wind turbine tower are controlled by the bending moment and axial force at the bottom; the performance of normal use should ensure that during operation the wind blade will not contact with the tower body. Therefore, displacements of wind blade and the top of tower were regarded as objective A and objective B, and the tower central axial force and basal moment were regarded as objective C and objective D, respectively (as shown in Fig. 1).

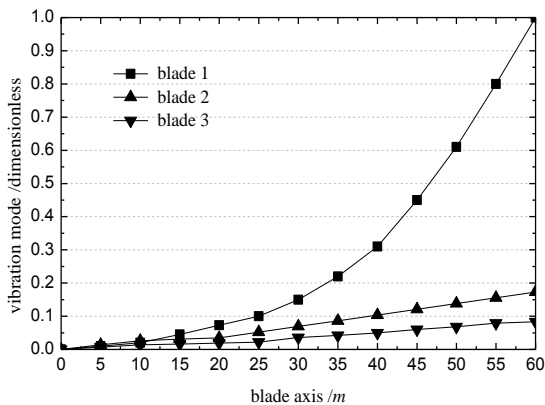
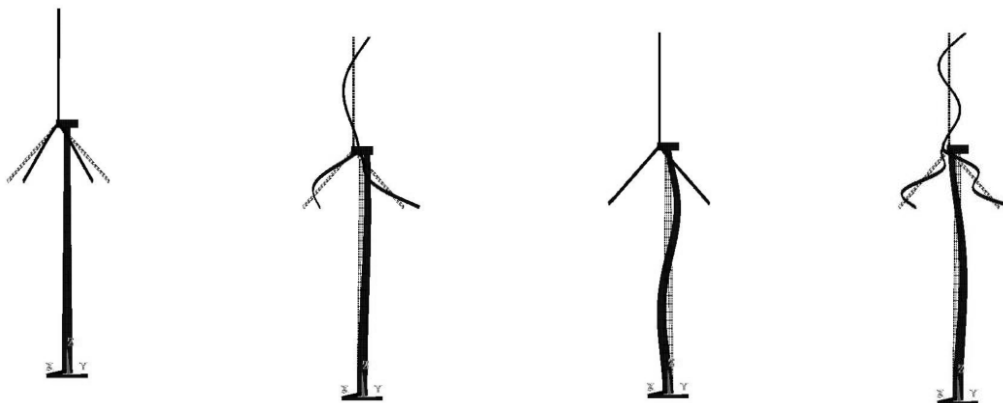


Fig. 3 The 1st mode of wind blades vibration



(a) The 1st modal shape (b) The 5th modal shape (c) The 30th modal shape (d) The 50th modal shape

Fig. 4 Typical vibration modes of tower-blade coupled wind turbine systems

Fig. 2 was shown that the distributions of the first 200 natural frequencies of the tower-blade coupled system considering or ignoring the centrifugal force effect, respectively. It was found that the fundamental frequency of tower-blade system with the centrifugal force effect was slightly larger than that without considering the effect of centrifugal force. Also, with the number of modal order increasing, the centrifugal force had a growing influence on the natural frequency. It also showed that the fundamental frequency of the system (0.27Hz) was very low, with the 50th modal frequency being 9.56Hz, and the interval between modal frequencies was very small.

Fig. 3 illustrated that the blade vibration based on the first mode. It showed that the vibration amplitude of a single wind blade was the largest, while that of 3 wind blades was the smallest. According to different modal shapes of the tower-blade coupled system based on the 1st, 5th, 30th, and 50th order modes presented in Fig. 4, it was obvious that the vibration modes with lower modal order were mainly in back-forth waving and left-right swinging of wind blades and the tower itself appeared structurally deformed and instable in modes with higher order, which were coupled with deformation of wind blades.

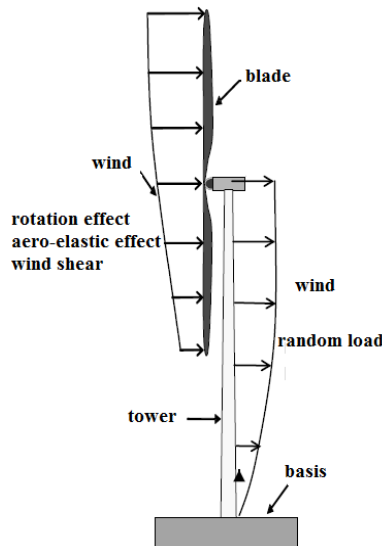


Fig. 5 Characteristics of wind turbine system

### 3. Simulation of random wind field of the tower-blade system

The fluctuating wind field of wind turbine system consists of two parts related to the tower and the blade, respectively. Fig. 5 showed characteristics of the wind field briefly. Wind fields of wind blade and tower interacted with each other when the wind turbine was in use. Especially, upwind blades in the wind direction had more obvious effects in the tower. More importantly, the wind field of wind blade was influenced by its rotation effect and modal and aerodynamic interference effects with the tower. As the tower was a conical structure, it was assumed that stiffness kept the same at all directions, and wind blades were always upwind, which made the lateral and vertical wind fields have little influence in the tower-blade system. The fluctuating wind energy along wind direction was the main load that the wind blade and the tower bear, so the numerical simulation of the along-wind fluctuating wind speed time series of the wind blade and the tower was mainly built in this paper.

#### 3.1 Simulation of fluctuating wind velocity of the tower

The incoming wind velocity time histories of the tower and the wind blade were simulated using the harmonic superposition method for numerical simulation of stationary random process, which was proposed by Shinozuka (1990), Ahsan (2008). Since blades and tower interacted with each other in three directions, the Davenport correlation coefficient (Davenport 2001)  $C_{ij}$  was introduced to consider the correlation between blades and tower

$$C_{ij} = \exp \left[ - \frac{\omega \sqrt{C_x (x_i - x_j)^2 + C_y (y_i - y_j)^2 + C_z (z_i - z_j)^2}}{2\pi v(H)} \right] \quad (1)$$

where  $C_x$ ,  $C_y$ , and  $C_z$  are respectively the transversal, downwind, and vertical attenuation

coefficients of any two points on the wind blades and the tower;  $\omega$  is the fluctuating wind frequency;  $v(H)$  is the average wind speed at the height of  $H$ . If the influence of correlation in only the vertical direction is considered, then  $C_x=C_y=0$ ,  $C_z=10$ . Under the fixed fluctuating wind frequency, the correlation between each point became smaller with the increase of the distance.

The Davenport level wind velocity spectrum was given by

$$\frac{nS(n)}{u_*^2} = \frac{4f^2}{(1+f^2)^{4/3}} \tag{2}$$

where  $n$  represents the simulated frequency value,  $f=1200n/U_{10}$ , and  $U_{10}$  represents the average wind speed at the height of ten meters.

Since wind can be considered as Gauss stationary processes, then  $n$  nodes for wind speed simulation in wind turbine system were defined, and stationary Gauss processes with zero mean were assumed. Matrix of the spectral density function was as following

$$S(\omega) = \begin{bmatrix} s_{11}(\omega) & s_{12}(\omega) & \dots & s_{1n}(\omega) \\ s_{21}(\omega) & s_{22}(\omega) & \dots & s_{2n}(\omega) \\ \dots & \dots & \dots & \dots \\ s_{n1}(\omega) & s_{n2}(\omega) & \dots & s_{nn}(\omega) \end{bmatrix} \tag{3}$$

where  $S_{ii}(\omega)$  is the auto-power spectrum of fluctuating wind at the node, calculated using the wind spectrum model in Eq. (2);  $S_{ij}(\omega)$  is the cross-power spectrum, the expression of which requires the coherence of any two points between the tower and the wind blade or between the tower and the tower, as shown in Eq. (4)

$$S_{ij}(\omega) = \sqrt{S_{ii}(\omega)S_{jj}(\omega)}C_{ij} \tag{4}$$

As for the wind blade, it's only needed to consider the coherence between each point inside the rotating plane. As for the wind blade and the tower, it's also needed to consider the coherence of along wind effects. Then the Cholesky decomposition was performed to  $S(\omega)$  as follows

$$S(\omega) = H(\omega) \cdot H^*(\omega)^T \tag{5}$$

In Eq. (5),  $H^*(\omega)^T$  is the conjugate transpose of  $H(\omega)$ . The three-dimensional matrix expression of  $H(\omega)$  is

$$H(\omega) = \begin{bmatrix} H_{11}(\omega) & 0 & \dots & 0 \\ H_{21}(\omega) & H_{22}(\omega) & \dots & 0 \\ \dots & \dots & \dots & \dots \\ H_{n1}(\omega) & H_{n2}(\omega) & \dots & H_{nn}(\omega) \end{bmatrix} \tag{6}$$

The fluctuating wind speed time series of any node on the wind power tower can be determined by its power spectrum. According to the harmonic superposition theory, the simulated wind speed time-history can be expressed as

$$v_j(t) = \sum_{m=1}^j \sum_{l=1}^N |H_{jm}(\omega_l)| \cdot \sqrt{2\Delta\omega} \cdot \cos[\omega_l t + \psi_{jm}(\omega_l) + \theta_{ml}] \quad j = 1,2,3 \dots n \tag{7}$$

In Eq. (7), the wind spectrum is divided into  $N$  equal parts in the frequency range;  $\Delta\omega$  equals to  $\omega/N$  and represents the increment of frequency;  $|H_{jm}(\omega_l)|$  represents the norm of the lower triangular matrix which is acquired by the Cholesky decomposition of the matrix of incoming wind spectrum;  $\theta_{ml}$  is a random number uniformly distributed between zero and  $2\pi$ , which is generated by Matlab;  $\omega_l$  equals to  $l \cdot \Delta\omega$  and represents the increment variable in the frequency domain;  $\psi_{jm}(\omega_l)$  represents the phase angle between two different action spots, which is determined by the ratio of the imaginary part of  $H_{jm}(\omega_l)$  and the real part of  $H_{jm}(\omega_l)$

$$\psi_{jm}(\omega_l) = \arctan\left(\frac{\text{Im}[H_{jm}(\omega_l)]}{\text{Re}[H_{jm}(\omega_l)]}\right) \tag{8}$$

In sum, the fluctuating wind velocity time history of the tower can be simulated by Eq. (7), which can take in account coherence effects of any nodes between wind blade and tower.

### 3.2 Simulation of fluctuating wind velocity of blades

Different from simulation of fluctuating wind field of the tower, as for simulation of wind speed in wind blades it's needed to consider rotational effect and elastic effect of the wind blades themselves. Currently there are three ways to solve aerodynamic performance of wind blades (Veers and Ashwill 2003): blade element-momentum theory, vortex wake method, and the CFD method. The vortex wake method is suitable to simulate the complex wind field, which is used to accurately calculate detailed wind load distribution on the blade. The vortex wake method needs smaller calculation amount than the CFD method, however, it cannot meet requirements of the fast calculation of wind turbine. The CFD method is the most accurate method to calculate aerodynamic characteristics of the wind blade, but the calculation amount is too large. So in this paper the modified blade element-momentum theory was adopted to simulate aerodynamic loads of the wind blade, and achieve two-way coupling of wind and blades.

Blade element-momentum is the most classic method to calculate aerodynamic loads of the wind turbine. In this paper, the modified blade element-momentum theory (Wang and Coton 2001, Wang *et al.* 2012) was adopted, which introduces the loss of blade root and tip, uses the empirical model of  $C_t$  when the axial inducible factor is bigger, and adds dynamic inflow and dynamic stall model into the simulation. Based on the modified blade element-momentum theory, dynamic loads of the wind turbine on conditions of different wind speed, speed of revolution, propeller pitch angle and drift angle can be calculated. Then the fluctuating wind velocity time history acted on the wind blade can be obtained. The specific method is as follows:

According to the blade element-momentum theory, the relative wind speed  $V_{rel}$  on the wind blade can be calculated by the following equation

$$\begin{pmatrix} v_{rel,x} \\ v_{rel,y} \end{pmatrix} = \begin{pmatrix} v_{ox} \\ v_{oy} \end{pmatrix} + \begin{pmatrix} 0 \\ v_{rot} \end{pmatrix} + \begin{pmatrix} W_x \\ W_y \end{pmatrix} - \begin{pmatrix} v_{bx} \\ v_{by} \end{pmatrix} \tag{9}$$

In Eq. (9),  $V_{ox}$  and  $V_{oy}$  are the flow pulsation wind speeds of downwind and crosswind respectively, which can be calculated by the harmonic superposition method in Eq. (7).  $V_{rot}$  represents the linear velocity caused by the rotation of the leaf blade,  $V_{bx}$  and  $V_{by}$  are vibrational speeds of the blade, and  $W$  represents induced velocity. Relationships of all speeds are as shown in Fig. 6.

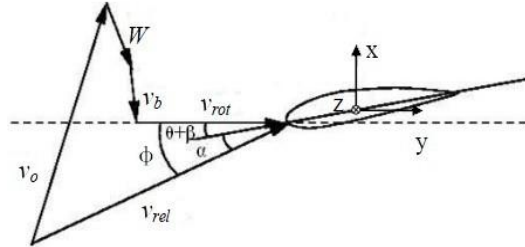


Fig. 6 The local velocity triangle through a wind blade

Induced velocity  $W$  can be expressed by following equations

$$\begin{cases} W_x = \frac{-BL \cos \phi}{4\rho\pi r F |v_0 + f_g n(nW)|} \\ W_y = \frac{-BL \sin \phi}{4\rho\pi r F |v_0 + f_g n(nW)|} \end{cases} \quad (10)$$

In Eq. (10),  $B$  represents the number of blades,  $L$  represents the lift force,  $\phi$  represents the up-flow angle,  $\rho$  represents the air density,  $r$  represents the span-wise location of the blade section,  $n$  represents the single order vector in the direction of propulsive force,  $F$  represents the Prandtl tip loss factor, and  $f_g$  represents the Glauert correction. Meanwhile the dynamic inflow model and dynamic stall model are adopted to correct the unsteady effect of the wind blade.

The angle of attack  $\alpha$  of the wind blade is calculated by

$$\alpha = \phi - (\beta + \theta_{twist}) \quad (11)$$

In Eq. (11),  $\beta$  represents the pitch angle, and  $\theta_{twist}$  represents the geometrical twist angle on the profile of the wind blade.  $\phi$  is calculated by

$$\tan \phi = \frac{v_{rel,x}}{v_{rel,y}} \quad (12)$$

Based on interpolation method, the wind turbine airfoil, the lift coefficient  $C_l$  and the drag coefficient  $C_d$  can be obtained, then the lift force  $L$  and the resistance  $D$  can be calculated by following equations

$$\begin{cases} L = 0.5\rho |v_{rel}|^2 C_l c \\ D = 0.5\rho |v_{rel}|^2 C_d c \end{cases} \quad (13)$$

Then the normal load  $F_n$  and the circumferential load  $F_t$  of the wind blade are given by

$$\begin{cases} F_n = L \cos \phi + D \sin \phi \\ F_t = L \sin \phi - D \cos \phi \end{cases} \quad (14)$$

In summary, firstly the program to simulate the wind velocity time history of the wind blade was written based on Eq. (7), induced velocities of each sample's wind velocity history were then calculated by Eq. (10). After repeating such cyclic calculations, the fluctuating wind velocity time

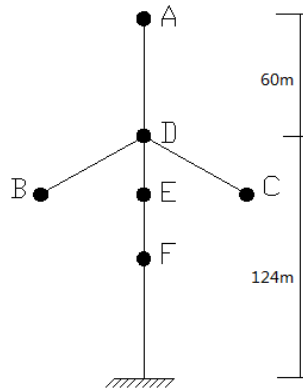
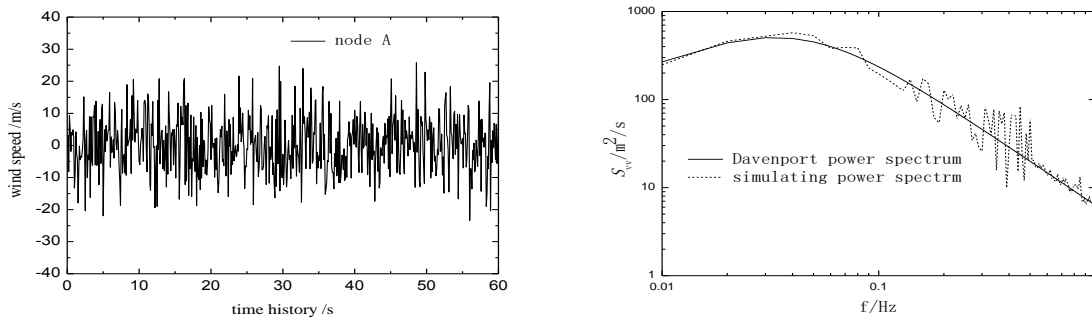


Fig. 7 Simplified simulating model and typical nodes of wind field



(a) The time curve of fluctuating wind

(b) The calibration curve of pulsating wind spectrum

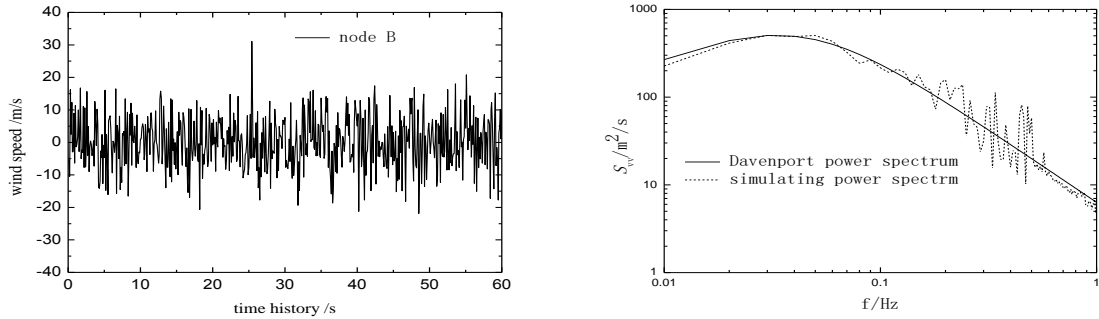
Fig. 8 Simulation results of fluctuating wind velocity at node A

history of the wind blade was obtained, as well as the lift coefficient and the drag coefficient of the wind blade. Then values of normal load and tangential load of the wind blade borne also were obtained finally.

### 3.3 Simulating results of the fluctuating wind velocity

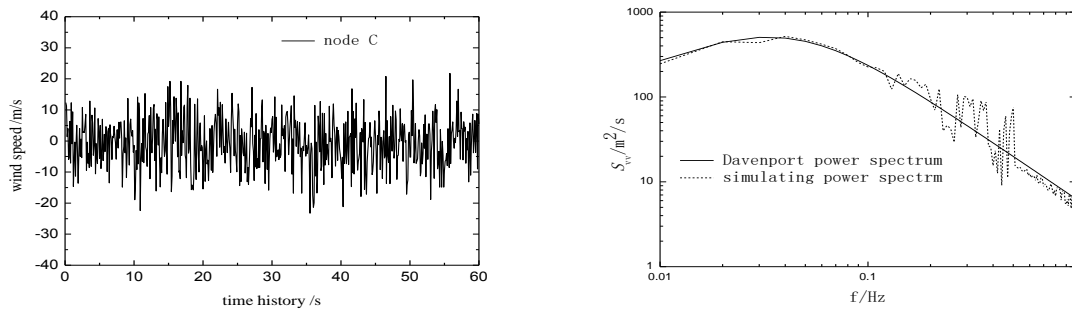
Take the 5 MW wind turbine system with three blades for instance. The Descartes coordinate system was adopted as the coordinate system, which sets its origin point at the center of the blade hub. As illustrated in Fig. 7, coordinate parameters of each point according to wind blades and the tower were calculated. Numerical simulating results of the fluctuating wind speed time history from point A to point F were presented directly in this paper due to the limit of space.

Based on the harmonic superposition method and modified blade element-momentum theory, during calculations in this paper, the upper limit frequency of pulsating wind was set as  $2\pi$ , the number of segmentation points of the fluctuating wind frequency was 2048, the increment of the frequency  $\Delta\omega$  was 0.00307 Hz, and the average wind speed of the local 10m height was 24 meters per second. Both the incoming wind velocity spectrum and coherence function adopted the Davenport wind spectrum model based on Eq. (1) and Eq. (2). The simulating time-history and the power spectrum curves of the fluctuating wind speed from point A to point F were showed in Figs.



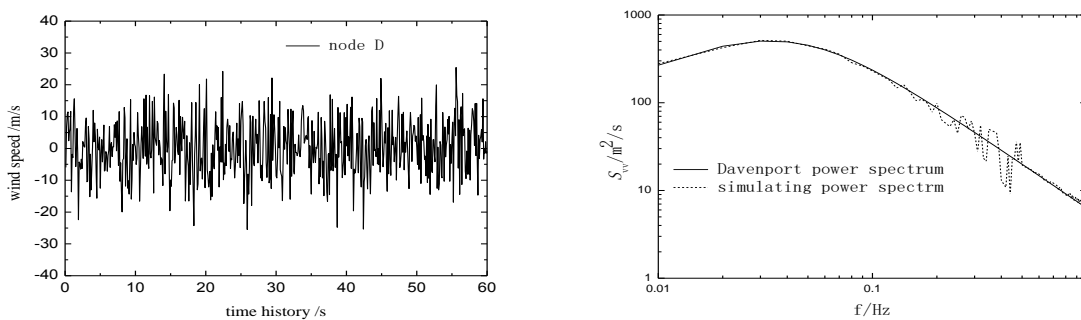
(a) The time curve of fluctuating wind (b) The calibration curve of pulsating wind spectrum

Fig. 9 Simulation results of fluctuating wind velocity at node B



(a) The time curve of fluctuating wind (b) The calibration curve of pulsating wind spectrum

Fig. 10 Simulation results of fluctuating wind velocity at node C



(a) The time curve of fluctuating wind (b) The calibration curve of pulsating wind spectrum

Fig. 11 Simulation results of fluctuating wind velocity at node D

8-13. In order to verify the correctness and obtain wind spectrum characteristics of the wind speed, coordinate systems for the calculated spectrum of the fluctuating wind velocity time history and the Davenport wind spectrum were logarithmic.

From the comparative analysis based on Figs. 8-13, the following conclusions could be obtained:

- (1) Curves of fluctuating wind power spectrum at point A, B and C on wind blades present

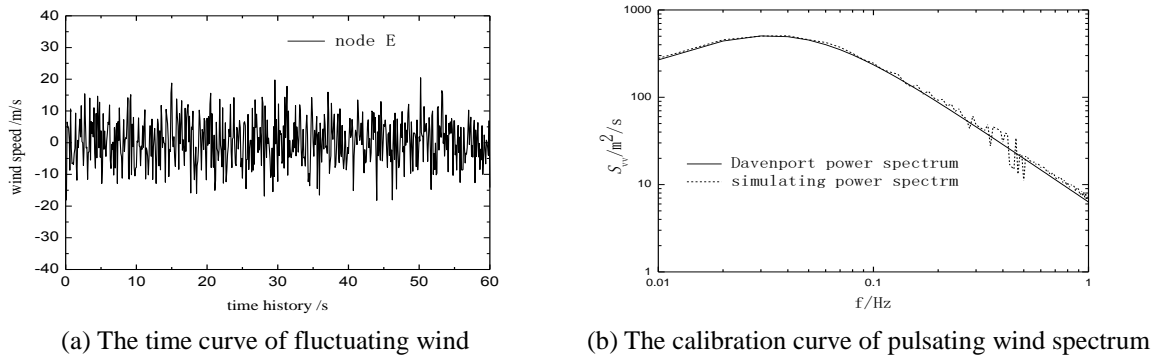


Fig. 12 Simulation results of fluctuating wind velocity at node E

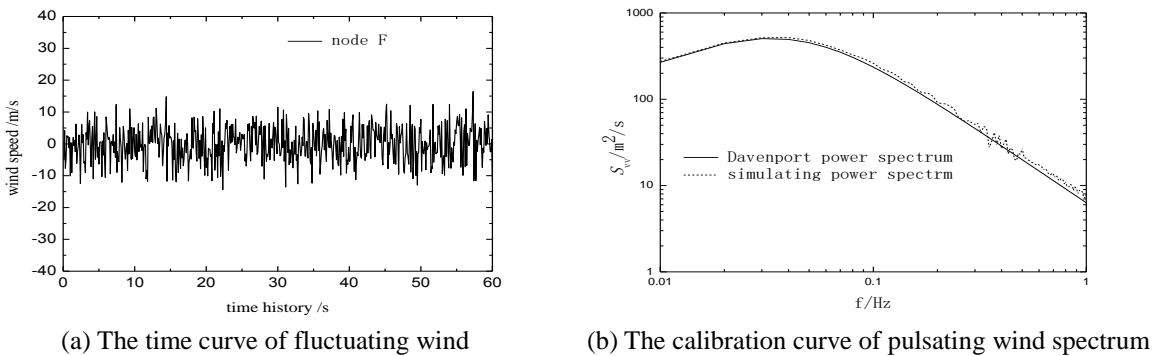


Fig. 13 Simulation results of fluctuating wind velocity at node F

large power radius and fluctuant range at high frequencies. The high frequency energy is caused by 3D rotation and interference effect between wind blades, which should be paid attention to in the analysis of wind-induced vibration in the wind turbine system;

(2) As for point *E* and *F*, which belong to the tower, there simulating curves of fluctuating wind speed have good agreements with the objective Davenport spectrums. Also, the energy floating and numerical value at high frequencies gradually reduce with the decreasing of height, since the simulating curve of wind speed at node *F* is basically consistent with Davenport spectrum;

(3) In conclusion, according to the simulating process and the comparative analysis, it can be found that the simulating method applied in this paper can precisely simulate the fluctuating wind velocity time history considering the rotation effect of the wind blades, and the coherence effect between wind blades and the tower.

Fig. 14 showed aerodynamic load distribution curves of the wind turbine in-plane and out-of-plane, Fig. 15 showed axial distribution curves of the wind blade lift force, drag force and the pitching moment coefficients. Then aerodynamic load characteristics of wind blades in large wind turbine system were analyzed based on Figs. 4-5. Fig. 4 showed that as for the wind blade, the numerical value of the out-of-plane aerodynamic load was far greater than that of the in-plane aerodynamic load, both of which increased first and then decreased along the wind blade shaft radius; the out-of-plane aerodynamic load increased more obviously than the in-plane aerodynamic

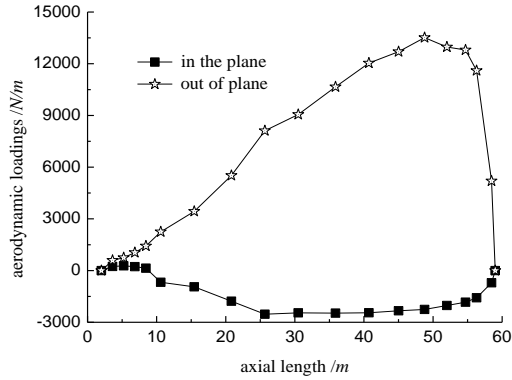


Fig. 14 The aerodynamic loads of blades

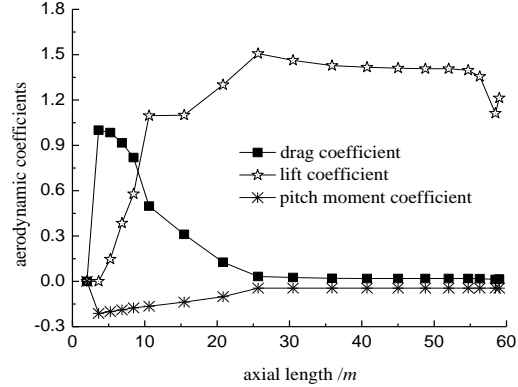


Fig. 15 The aerodynamic load coefficients of blades

load. Fig. 5 showed that, as for the wind blade, aerodynamic lift coefficient was greater than resistance coefficient and pitching moment coefficient, which three coefficients all increased rapidly along the axial radius and gradually approached to plateaus near the midpoint of the wind blade.

#### 4. Introduction of MCCM

The consistent coupling method (CCM) was put forward by the author (Ke and Ge 2012), which method is used to calculate wind-induced responses of flexible structures, considering the background component, resonance component and the cross terms between background and resonance. In this paper, the modified “consistent coupling method” (MCCM) was introduced to consider the modal coupling between the wind blade and tower, and the coupling effect among all the resonant modes of the system.

The dynamic response of a wind turbine system to the turbulent wind excitation can be expressed in terms of the matrix equations as follows

$$[M]\{\ddot{y}\} + [C]\{\dot{y}\} + [K]\{y\} = [T]\{p(t)\} \tag{16}$$

where  $p$  means external stochastic wind load vector;  $M$ ,  $C$  and  $K$  mean the mass, damping and stiffness matrix, respectively, and  $T$  means the force indicating matrix that is used to match dimension numbers of node number and external wind load vector.

Using the modal coordinate systems, the wind-induced dynamic displacement can be represented as

$$\{y(t)\} = \Phi \{q(t)\} = \sum_{i=1}^m \phi_i q_i(t) + \sum_{i=m+1}^n \phi_i q_i(t) = \{y\}_d + \{y\}_s \tag{16}$$

where  $y_d$  is the response considering the background and resonant contributions of former  $m$  modes,  $y_s$  is the response only considering quasi-static contribution of remaining modes,  $q$  is the generalized displacement vector, and  $\Phi$  is the vibration matrix of modes.

The dynamic response is  $K^{-1}P$  under the wind load  $P$ , which can be unfolded as

$$[K]^{-1}\{p(t)\} = \sum_{i=1}^n [F]_i \{p(t)\} = \sum_{i=1}^m [F]_i \{p(t)\} + \sum_{i=m+1}^n [F]_i \{p(t)\} \tag{17}$$

where  $F_i$  is the flexibility matrix of the  $i_{th}$  mode, given by

$$[F]_i = \frac{\{\phi\}_i \{\phi\}_i^T}{\{\phi\}_i^T [K] \{\phi\}_i} \tag{18}$$

And  $y_s$  can be expressed as

$$\{y\}_s = \sum_{i=m+1}^n [F]_i \{p(t)\} = [K]^{-1}\{p(t)\} - \sum_{i=1}^m [F]_i \{p(t)\} \tag{19}$$

Combining Eq. (16) and Eq. (19), then dynamic response  $y$  can be expressed as

$$\begin{aligned} \{y(t)\} &= \{y\}_d + \{y\}_s = \sum_{i=1}^m \phi_i q_i(t) + [K]^{-1}\{p(t)\} - \sum_{i=1}^m [F]_i \{p(t)\} \\ &= \sum_{i=1}^m (\phi_i q_i(t) - [F]_i \{p(t)\}) + [K]^{-1}\{p(t)\} \end{aligned} \tag{20}$$

Accordingly, the background and resonant responses are given by

$$\{y(t)\}_b = [K]^{-1}\{p(t)\} \tag{21}$$

$$\{y(t)\}_r = \sum_{i=1}^m (\phi_i q_i(t) - [F]_i \{p(t)\}) \tag{22}$$

And  $\sigma_t$  is the root-mean-square (RMS) value of dynamic response  $y$ , expressed by

$$\sigma_t = \sqrt{\sigma_r^2 + \sigma_b^2 + 2\rho_{r,b}\sigma_r\sigma_b} = \sqrt{\sigma_r^2 + \sigma_b^2 + \sigma_c^2} \tag{23}$$

where  $\sigma_b$ ,  $\sigma_r$  and  $\sigma_c$  are response component vectors of background, resonant and coupled term, respectively.  $\rho_{r,b}$  is the correlation coefficient between background and resonant components, given by

$$\rho_{r,b} = \frac{\sigma_{r,b}}{\sigma_r\sigma_b} = \frac{\int \sum_{j=1}^n \sum_{k=1}^n \phi_{j,i} \phi_{k,i} S_{q_{b,j}, q_{r,k}}(\omega) d\omega}{\text{sqrt}(\int \sum_{j=1}^n \sum_{k=1}^n \phi_{j,i} \phi_{k,i} S_{q_{r,j}, q_{r,k}}(\omega) d\omega) \int \sum_{j=1}^n \sum_{k=1}^n \phi_{j,i} \phi_{k,i} S_{q_{b,j}, q_{b,k}}(\omega) d\omega)} \tag{24}$$

It can be found in Eq. (23) that fluctuating wind-induced responses of wind turbine system should include background, resonant and coupled components between the former two terms. However, the tri-component method based on SRSS combination cannot consider the coupled component, which is acceptable for the small value of  $\rho_{r,b}$ , but widely different for some through coupled structures. Due to the complex calculation process of Eq. (24), the approach of solving coupled component based on covariance matrix of coupled restoring force was presented in this paper.

#### 4.1 Covariance matrix of resonant (background, coupled) elastic restoring force

The generalized displacement response of the  $i_{th}$  mode only containing the resonant component from Eq. (22) is given by

$$q_{r,i}(t) = q_i(t) - \frac{\phi_i^T \{p(t)\}}{\phi_i^T [K] \phi_i} = q_i(t) - \frac{F_i(t)}{K_i} \quad (25)$$

Accordingly, the cross-power spectrum of generalized resonant displacement between the  $i_{th}$  mode and the  $j_{th}$  mode is expressed as

$$\begin{aligned} S_{q_{r,i}, q_{r,j}}(\omega) &= \int_{-\infty}^{\infty} R_{q_{r,i}, q_{r,j}}(\tau) e^{-i2\pi\omega\tau} d\tau = \int_{-\infty}^{\infty} E[q_{r,i}(t), q_{r,j}(t+\tau)] e^{-i2\pi\omega\tau} d\tau \\ &= (H_i^*(\omega) - \frac{1}{K_i})(H_j(\omega) - \frac{1}{K_j}) S_{F_i, F_j}(\omega) = H_{r,i}^*(\omega) H_{r,j}(\omega) S_{F_i, F_j}(\omega) \end{aligned} \quad (26)$$

where  $H_{r,i} = H_i(\omega) - 1/K_i$ , which is the resonant transfer function of the  $i_{th}$  mode.  $K_i$  is the stiffness matrix of the  $i_{th}$  mode, which can be expressed as

$$[K]_i = \frac{\{\phi\}_i^T [K] \{\phi\}_i}{\{\phi\}_i \{\phi\}_i^T} \quad (27)$$

The covariance matrix of generalized resonant response is given by

$$[C_{qq}]_r = \int_{-\infty}^{\infty} H_r^* S_{FF} H_r d\omega = \int_{-\infty}^{\infty} H_r^* \Phi^T T D S_{AA} D^T T^T \Phi H_r d\omega \quad (28)$$

where  $A$  and  $D$  are time coordinate vector and proper mode matrix with Proper orthogonal decomposition (POD) method, respectively. Because the dimension number of  $p(t)$  is very large, so the POD method is used to reduce the dimension number of  $p(t)$  to save computing time. And accordingly, the resonant elastic restoring force vector can be represented as

$$\{P_{qq}\}_r = [K] \{y(t)\}_r = [K][\Phi] \{q(t)\}_r = [M][\Phi][\Lambda] \{q(t)\}_r \quad (29)$$

The cross-covariance matrix  $[C_{pp}]_r$  of  $\{P_{qq}\}_r$  is expressed as

$$\begin{aligned} [C_{pp}]_r &= \overline{\{P_{qq}\}_r \{P_{qq}\}_r^T} = [M][\Phi][\Lambda] \overline{\{q(t)\}_r \{q(t)\}_r^T} [\Lambda]^T [\Phi]^T [M]^T \\ &= [M][\Phi][\Lambda] [C_{qq}]_r [\Lambda]^T [\Phi]^T [M]^T \end{aligned} \quad (30)$$

From Eq. (28) and Eq. (29), it can be easily found that the accuracy of  $P_{eqq,r}$  is determined by the number of calculating modes and dynamic characteristics of the structure, and the covariance matrix of total fluctuating elastic restoring force  $C_{pp,i}$ , can be obtained by Eq. (30) as long as resonant transfer function  $H_r$  is replaced by generalized transfer function  $H$ . In this paper, in order to calculate coupled component, the covariance matrix of coupled elastic restoring force  $C_{pp,c}$  was defined as following

$$[C_{pp}]_c = [C_{pp}]_t - ([C_{pp}]_b + [C_{pp}]_r) \quad (31)$$

#### 4.2 Wind-induced response of resonant, background and cross terms

It is clear that the resonant and coupled responses can be regarded as the quasi-static responses under the inertial load excitation. Thus, the resonant and coupled responses can be obtained using Load-response-correlation (LRC) method (Kasperski 1992). Take the resonant component for example, an arbitrary dynamic response of interest  $r(t)$  is given by

$$\{r(t)\}_r = [I] \{P_{eqq}\}_r \tag{32}$$

And the covariance matrix of resonant response  $r(t)$  is expressed as

$$[C_{rr}]_r = \overline{\{r(t)\}_r \{r(t)\}_r^T} = [I] [C_{pp}]_r [I]^T = [I] [M] [\Phi] [\Lambda] [C_{qq}]_r [\Lambda]^T [\Phi]^T [M]^T [I]^T \tag{33}$$

where  $\Lambda = \text{diag}(\omega_1^2, \dots, \omega_m^2)$ . The RMS value vector of resonant response is given by

$$\sigma_{R,r} = \sqrt{\text{diag}([C_{rr}]_r)} \tag{34}$$

where  $\text{diag}(\cdot)$  is the column vector of diagonal elements of  $[C_{rr}]_r$ .

Accordingly, if the  $C_{rr,r}$  is replaced with  $C_{rr,b}$ ,  $C_{rr,c}$ , and  $C_{rr,t}$ , background, coupled and total fluctuating wind-induced response can be respectively obtained in the same way. It is worth noting that the value of covariance matrix of coupled component using Eq. (33) might be negative, which indicates that calculation with tri-component method will overrate the value of response. Hence, absolute value of these elements of  $C_{rr,c}$  should be adopted in Eq. (34), while in combination of total response the influence of negative value must be considered.

#### 4.3 Combination method

The total fluctuating response can be given by

$$\sigma_t = \sqrt{\sigma_r^2 + \sigma_b^2 + \text{sign}(\text{diag}([C_{rr}]_c)) \sigma_c^2} \tag{35}$$

Accordingly, the totally response of wind turbine system is then given by

$$R_a = \bar{R} + g \times \sqrt{\sigma_r^2 + \sigma_b^2 + \text{sign}(\text{diag}([C_{rr}]_c)) \sigma_c^2} \tag{36}$$

where  $R_a$  is the total wind-induced response which contains the mean term, background term, resonant term and cross term. And  $g$  is the peak factor, which is expressed by

$$g = \sqrt{2 \ln vT} + \frac{\gamma}{\sqrt{2 \ln vT}} \tag{37}$$

where  $T=600$  s, and  $\gamma$  is the Euler's constant, which is 0.5772.

### 5. Wind-induced responses and ESWL analysis

Figs. 16-17 showed that the power spectral density function curves of the objective A (wind

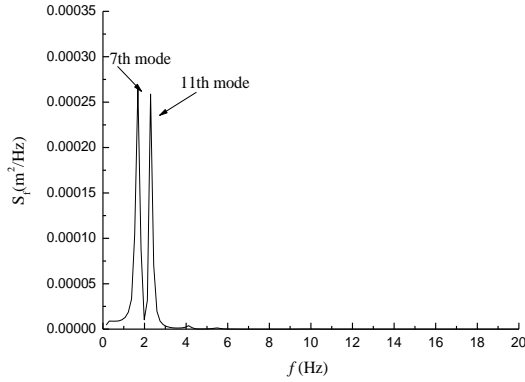


Fig. 16 PSD of displacement responses for node A

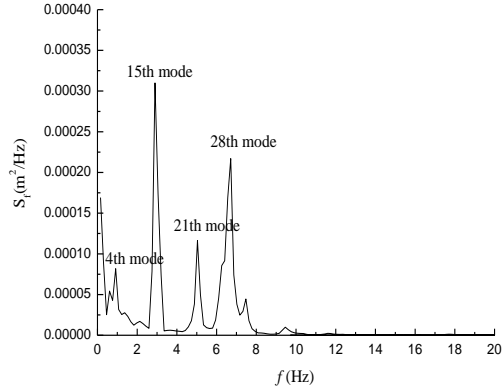


Fig. 17 PSD of displacement responses for node B

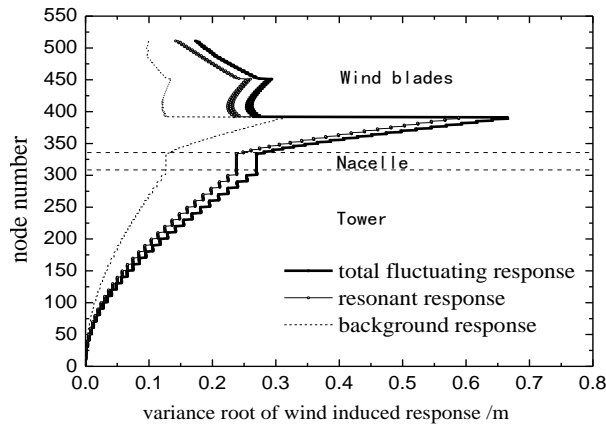


Fig. 18 The fluctuating wind-induced responses and components

blade displacement) and objective *B* (the tower top displacement) responses. It was found that the wind-induced response of the wind turbine tower-blade system mainly consisted of the background response of all the modal contribution, and the resonant response of special modal excitation. It was noted that the resonant effect caused by high order modes was very significant. For example, the displacement of wind blade was mainly caused by the resonance effect of the 7<sup>th</sup> and 11<sup>th</sup> order modes, while the local vibration was mainly caused by the corresponding mode; the energy contribution from the 1<sup>st</sup> mode of the tower top displacement response was very small, and the energy was mainly contributed by the 15<sup>th</sup>, 21<sup>st</sup> and 28<sup>th</sup> order modes, among which contribution from the 15<sup>th</sup> mode was the maximum. Analysis showed that wind-induced responses of the tower obviously were coupled with the wind blade modes, therefore the resonance effect of the higher order modes and the coupling terms between modes should not be ignored.

Fig. 18 was shown that the distribution curves of wind-induced background, resonant component and total fluctuating response of the wind turbine system. Fig. 19 extracted and showed the background, resonant component and cross terms of the wind-induced responses from objective A to objective D. Main conclusions based on Figs. 18-19 were drawn as follows:

- (1) With the increase of the tower height, the wind-induced background, resonant and total

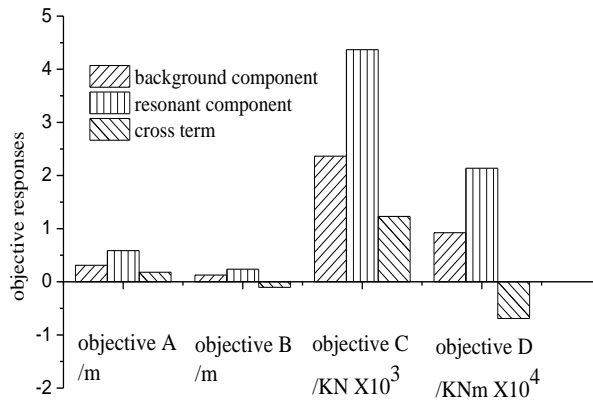


Fig. 19 The respective components for typical nodes

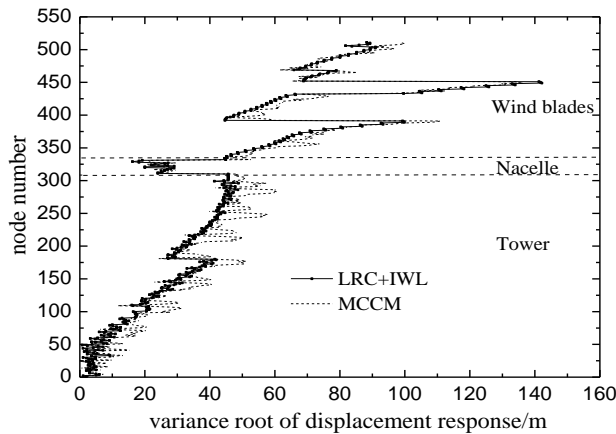


Fig. 20 ESWLs obtained by different calculating methods

fluctuating response of tower gradually increased, while the wind-induced response value of the nacelle kept relatively stable. Wind vibration responses of three wind blades in operating state were significantly different, patterns of which were inconsistent;

(2) The contribution of the background and resonant components of the wind turbine system cannot be ignored. These two components appeared with different proportion in different regions. The resonant components were dominant in all regions. The background and coupling components were in the same orders of magnitude, but sometimes the coupling terms were negative (negative value indicated that the response of structure was overestimated by ignoring coupling terms in calculation), which cannot be ignored in the calculation of wind-induced responses for large wind turbine system.

Fig. 20 illustrated that the ESWL distribution curves calculated by the MCCM method and traditional method of three components (IWL+LRC, without considering the coupling effect between resonant modes and the effect of the cross term between the background and resonant modes). Fig. 21 showed ESWL distribution curves of the wind turbine system under different equivalent objectives. Then the ESWL distribution pattern of the wind turbine tower-blade system

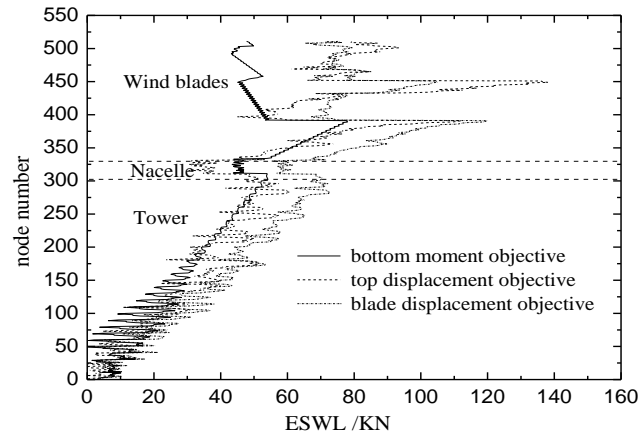


Fig. 21 ESWLs aimed at different objectives

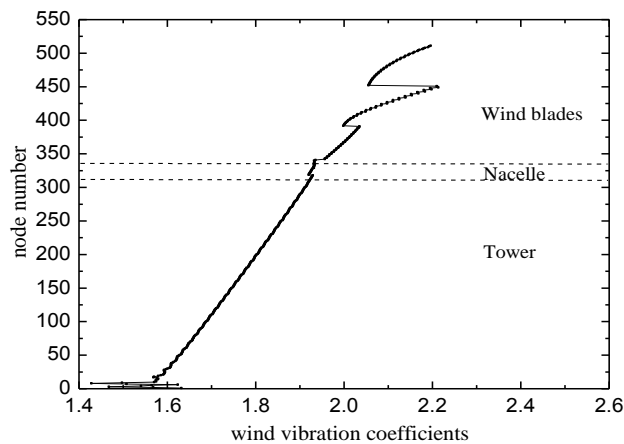


Fig. 22 Wind vibration coefficients of wind turbine tower-blade system

can be obtained based on Figs. 20-21.

Values of ESWL calculated by the MCCM were generally larger than results calculated by the traditional method LRC+IWL, which indicated that the calculation of ESWL of the wind turbine tower-blade system should consider the coupling effects between the resonant modes and the effect of the cross term between the background and resonant modes. ESWL values obtained based on three equivalent objectives and their distribution patterns were considerably different from each other. The ESWL value which regarded the bottom moment of the tower as the equivalent objective was relatively minimal, while ESWL values which respectively regarded the displacement of wind blade and that of the top tower as the equivalent objective distributes comparatively similar to each other. Therefore the ESWL pattern should be reasonably adopted according to design objectives of different stages in the design.

Wind vibration coefficient is a key parameter of the wind-resistant design in structures, compared to ESWL which is more suitable for engineering designer to use. Fig. 22 showed the distribution curve of the wind vibration coefficient based on the wind-induced displacement

responses of the wind turbine system. It was obviously found that the wind vibration coefficient fluctuated significantly at different parts. Hence, it was irrational to consider the wind vibration coefficient as a constant. With the increase of the tower height, wind vibration coefficients gradually increased in the whole. The wind vibration coefficient of nacelle was obviously smaller than those of three wind blades, wind vibration coefficients of which were also different from each other. The wind vibration coefficient of the upper wind blade was obviously larger than those values of the two lower wind blades, but as the wind blades were in the non-stop rotation, every wind blade should use its maximum wind vibration coefficient for wind-resistant design. In short, it was suggested that the different wind vibration coefficient should be adopted in different regions during the wind-resistant design of the wind turbine tower-blade system.

## **6. Conclusions**

In this paper the integration model of the large wind turbine system, the simulation of the fluctuating wind velocity of tower-blade system, the distribution characteristics of the wind-induced responses, and wind vibration coefficients were systematically discussed in this study.

- The effect of centrifugal force caused by the rotation of wind blades increases the stiffness of the wind turbine tower-blade system, which effect is much greater in modes with higher orders. The vibration mode of system with lower order is mainly in back-forth waving and left-right swinging of wind blades. Tower itself appears structurally deformed and instable in modes with high orders, which are coupled with deformation of wind blades.

- Fluctuating wind loads of the wind turbine system could be simulated precisely with harmonic superposition method and the modified blade element-momentum theory. The fluctuating wind velocity spectrum of wind blades appears energy concentration and larger fluctuation at higher frequency, but the fluctuating wind velocity spectrum of tower suffers from less interference effect of wind blades with the decrease of height, the simulating result of which is closer to the natural wind spectrum. Simulating results can provide input parameters for the analysis of wind-induced dynamic response of the wind turbine system.

- The wind-induced vibration of large tower-blade coupled wind turbine system appears three main characteristics, which are complicated modal responses, multi-mode coupling effect, and multiple equivalent objectives. The resonant effect is dominant at the upper part of the tower and wind blades, while the background component is similar to the resonant component at the bottom of the tower.

- The ESWL distribution patterns aimed at different equivalent objectives of large tower-blade coupled wind turbine system vary considerably. Appropriate ESWL distribution pattern should be selected according to the design process. The distribution regularity of wind vibration coefficients is obvious. The wind vibration coefficient has the maximum value in wind blades, becomes stable in the nacelle, while increases gradually in the tower with the increase of the height.

## **Acknowledgments**

The research described in this paper was financially supported by National Basic Research Program of China (2014CB046200), National Natural Science Foundation (50978203, 51208254), Jiangsu Province Natural Science Foundation (BK2012390) and China Postdoctoral Science

Foundation (2013M530255), which are gratefully acknowledged.

## References

- Agarwal, P. and Manuel, L. (2009), "Simulation of offshore wind turbine response for long-term extreme load prediction", *Eng. Struct.*, **31**(10), 2236-2246.
- Ahsan, K. (2008), "Numerical simulation of wind effects: a probabilistic perspective", *J. Wind Eng. Ind. Aerodyn.*, **96**(10), 1472-1497
- Burton, T., Sharpe, D. and Jenkins, N. (2011), *Wind Energy Handbook*, John Wiley&Sons, Chichester, England.
- Cheng, P.W. (2002), "A reliability based design methodology for extreme response of offshore wind turbine", Wind Energy Research Institute, Delft University of Technology, Netherlands
- Duquette, M.M. and Visser, K.D. (2003), "Numerical implications of solidity and blade number on rotor performance of horizontal-axis wind turbines", *J. Solar Energy Eng.*, **125**(4), 425-432.
- Germanischer Lloyd (2005), "GL-2005 Rules and guidelines IV-industrial services, part 2-guideline for the certification of offshore wind turbines", Germanischer Lloyd, Hamburg.
- He, G.L. and Li, J. (2011), "Stochastic dynamic response of wind turbine systems under wind loads", *J. Vib. Eng.*, **24**(6), 696-703. (in Chinese)
- Holm-Jørgensen, K., Larsen, J.W. and Nielsen, S.R.K. (2008), "On the nonlinear structural analysis of wind turbine blades using reduced degree-of-freedom models", *Struct. Eng. Mech.*, **28**(1), 107-127.
- Hsu, M.H. (2008), "Dynamic behaviour of wind turbine blades", *Proceedings of the Institution of Mechanical Engineers, Part C:Journal of Mechanical Engineering Science*, **222**(8), 1453-1464.
- Holmes, J. (2002), "Effective static load distributions in wind engineering", *J. Wind Eng. Ind. Aerodyn.*, **90**(2), 91-109.
- Katsumura, A., Tamura, Y. and Nakamura, O. (2007), "Universal wind load distribution simultaneously reproducing largest load effects in all subject members on large-span cantilevered roof", *J. Wind Eng. Ind. Aerodyn.*, **95**(9), 1145-1165.
- Karimirad, M. and Moan, T. (2011), "Wave-and wind-induced dynamic response of a spar-type offshore wind turbine", *J. Waterw., Port, Coastal, Ocean Eng.*, **138**(1), 9-20.
- Kasperski, M. and Niemann, H. (1992), "The LRC (load-response-correlation)-method a general method of estimating unfavourable wind load distributions for linear and non-linear structural behavior". *J. Wind Eng. Ind. Aerodyn.*, **43**(1), 1753-1763.
- Liao, M.F. (2008), *Wind Turbine Technologies*, The Northwest Industry University Press, Xi'an, China. (in Chinese)
- International Electrotechnical Commission (2006), *Wind Turbine Generator Systems-1: Design Requirements*, International Standard, Geneva, Switzerland.
- Murtagh, P.J., Basu, B. and Broderick, B.M. (2005), "Along-wind response of a wind turbine tower with blade coupling subjected to rotationally sampled wind loading", *Eng. Struct.*, **27**(8), 1209-1219.
- Petrini, F., Li, H. and Bontempi, F. (2010), "Basis of design and numerical modeling of offshore wind turbines", *Struct. Eng. Mech.*, **36**(5), 599-618.
- Shinozuka, M. and Seya, H. (1990), "Stochastic methods in wind engineering", *J. Wind Eng. Ind. Aerodyn.*, **36**(2), 1472-1497
- Ke, S.T., Ge, Y.J., Zhao, L. and Tamura, Y. (2012), "A new methodology for analysis of equivalent static wind loads on super-large cooling towers". *J. Wind Eng. Ind. Aerodyn.*, **111**(3), 30-39
- Tarp, J., Madsen, P.H. and Frandsen, S. (2002), "Partial safety factors in the 3rd edition of IEC 61400 1: wind turbine generator systems-part 1: safety requirements", Technical Report R-1319, Riso National Laboratory, Roskilde
- Tempel, J.V.D. (2006), "Design of support structures for offshore wind turbines", Delft University of Technology, Netherlands.

- Veers, P.S., Ashwill, T.D., Sutherland, H.J. *et al.* (2003), "Trends in the design, manufacture and evaluation of wind turbine rotor", *Wind Energy*, **6**(3), 245-259.
- Wang, T.G. and Cotton, F.N. (2000), "Prediction of the unsteady aerodynamic characteristics of horizontal-axis wind turbines including three-dimensional effects", *Proceedings of the Institution of Mechanical Engineers Part A: Journal of Power and Energy*, **214**(5), 385-400
- Wang, T.G., Wang, L., Zhong, W. *et al.* (2012), "Large-scale wind turbine blade design and aerodynamic analysis", *Chinese Sci. Bul.*, **57**(5), 466-472.

CC